Influence of roughness filters in the analysis of elastohydrodynamic and dry circular contact

Pedro Romio[1], Miguel Correia[1], João Marafona[1]

[1]*Dept. of Mechanical Engineering, University of Porto*
R. Dr. Roberto Frias, 4200-465, Porto, Portugal
pedroromio@fe.up.pt

Abstract. Surface finishing and roughness parameters can directly affect the system's efficiency and components' useful life of several mechanical applications. In order to evaluate these parameters' influence, one can employ numerical methods that predict the pressure field and maximum contact pressure. The problem assessed in this study is that, despite surface roughness being an "intrinsic" surface property, measured roughness is "extrinsic" meaning that instruments using different sampling intervals and filters produce different asperities distribution, which can affect the pressure field predicted by numerical modelling. Therefore, this study employs two numerical models, a Dry Circular Contact (DCC) model and an Elastohydrodynamic lubrication (EHL) model to investigate filtering influence over the maximum contact pressure. The results show that the same surface filtered with different cut-off lengths presents distinct pressure fields and maximum pressure values. Also, the simulations indicate that smaller cut-offs tend to produce higher pressures.

Keywords: Dry Circular Contact model, Elastohydrodynamic lubrication contact model, roughness and standardised cut-off lengths.

1 Introduction

Rolling element bearings, gears and cam followers are examples of machine parts whose operating principle is based on surface contact [1]. Consequently, their surface finishing and roughness parameters are expected to affect the system's efficiency and components' useful life. Nevertheless, describing the influence of these features and what happens inside the contact, namely the pressure field distribution, is not a simple task and is mainly done by resourcing to numerical methods [2].

That said, two numerical models for rough surfaces are evaluated in this paper: a Dry Circular Contact (DCC) model [3], used to describe the contact behaviour without lubrication, and an Elastohydrodynamic lubrication (EHL) model for circular contact [4], where a lubricant is introduced to separate the surfaces, minimising the solid/solid interaction.

Both models assume that the surfaces in contact can be expressed by a matrix containing the roughness's z coordinates, $s_1(x, y)$ and $s_2(x, y)$. The problem evaluated in this study is that, despite surface roughness being an "intrinsic" surface property, measured roughness is "extrinsic", which means that instruments using different sampling intervals and filters produce different asperities distribution [5], which can affect the pressure field predicted by numerical modelling. In other words, the exactly same surface, using different filters, can produce distinct pressure predictions.

In order to investigate the possible variations in the pressure field prediction, three distingue top-milling surfaces are measured using different cut-off lengths (λ_c) and the respective roughness matrices used in simulations to determine the maximum pressure under the same operational conditions. The results show that the same surface filtered with different cut-off lengths presents distinct pressure fields and maximum pressure values. Also, the simulations indicate that smaller cut-offs tend to produce higher pressures in both models.

2 Numerical modelling

2.1 Dry Circular Contact model

The DCC model used in this study is the same one presented by Sainsot and Lubrecht [3] and is employed to solve the complementarity problem shown in Equation (1).

$$\begin{aligned} h(x,y) > 0; \quad p(x,y) \leq 0 \quad \text{no contact} \\ h(x,y) = 0; \quad p(x,y) > 0 \quad \text{contact} \end{aligned} \tag{1}$$

The gap geometry $h(x,y)$ between the two bodies in contact can be expressed by Equation (2), where one can notice the terms $s_1(x,y)$ and $s_2(x,y)$ used to describe the surfaces' roughness.

$$h(x,y) = h_0 + \frac{x^2}{2R_x} + \frac{y^2}{2R_y} + u_z(x,y) + s_1(x,y) + s_2(x,y) \tag{2}$$

In addition, the pressure-induced elastic displacement $u_z(x,y)$ is given by Equation (3), and the load balance is expressed in Equation (4).

$$u_z(x,y) = \frac{1}{\pi \cdot E^*} \iint_A \frac{p(x',y')\ dx'dy'}{\sqrt{(x-x')^2 + (y-y')^2}} \tag{3}$$

$$\iint_A p(x,y)\ dx\ dy = P \tag{4}$$

The numerical approach used to solve Equations (1) to (4) simultaneously is well discussed in [3], and it allows one to obtain the pressure field distribution, as well as its maximum value in each simulation.

2.2 Elastohydrodynamic lubrication model

Six equations can mathematically define the EHL contact: (i) Reynolds equation, presented in Equation (5); (ii) gap geometry in Equation (2); (iii) pressure-induced elastic displacement shown in Equation (3), (iv) load balance from Equation (4), (v) density as a pressure and temperature function given by Equation (6) and (vi) viscosity as a pressure and temperature function in Equation (7) [4, 6 – 8].

$$\frac{\partial}{\partial x}\left(\frac{\rho \cdot h^3}{12 \cdot \eta \cdot \|\vec{v}_e\|}\frac{\partial p}{\partial x}\right) + \frac{\partial}{\partial y}\left(\frac{\rho \cdot h^3}{12 \cdot \eta \cdot \|\vec{v}_e\|}\frac{\partial p}{\partial y}\right) = \frac{\partial(\rho \cdot h)}{\partial y} \tag{5}$$

$$\rho = \rho_0 \cdot [1 + \gamma_t \cdot (T_0 - T)]\left(1 + \frac{C_a \cdot p}{1 + C_b \cdot p}\right) \tag{6}$$

$$\eta = \xi \cdot e^{\left(\frac{\zeta}{T+\psi}\right)} \cdot e^{(\alpha_{Gold} \cdot p)} \tag{7}$$

A thorough explanation of how to solve the system of equations using the semi-system approach is given by Wang et al. [4] and was used in this paper to obtain the pressure field distribution, as well as its maximum value in each simulation.

3 Roughness parameters

It is well known that every surface comprises different classes of irregularities, such as error form, waviness and roughness. The difference between roughness and waviness is related to the surface wavelength, and the point at which the roughness becomes waviness (the cut-off point) is arbitrary. Usually, the cut-off is expressed as a length and allows one to divide a composite surface in terms of roughness peaks and waviness peaks. The cut-off choice is related to the surface itself and can follow the recommendations in DIN 4768 [9]. This study uses three different standardised cut-off lengths (λ_c) to treat the measured surfaces: 0.08 mm, 0.25 mm and 0.80 mm.

In order to characterise the surfaces, four areal roughness parameters were evaluated [10]:

- Arithmetical Mean Height (S_a): defined as the arithmetic mean of the absolute value of the height within a sampling area;

- Root Mean Square Height (S_q): defined as the root mean square value of the surface departures z within the sampling area;
- Maximum Peak Height (S_p): defined as the height of the highest point of the surface;
- Maximum Height (S_z): defined as the difference between the surface's highest point and the surface's lowest point.

4 Materials and Methods

4.1 Samples manufacturing

Three different surfaces were manufactured using a top-milling process on a steel base material. The cutting speed was kept constant and equal to 200 m/min while the feed speed varied, as indicated in Table 1.

Table 1 - Feed speed used for samples manufacturing.

Surface sample	**1**	**2**	**3**
Feed speed (mm/min)	400	900	1600

4.2 Roughness evaluation

The roughness areas used in this study were acquired using 3D Optical Profilometer equipment (Bruker NPFLEX™, Germany, 2013). A 5 mm x 5 mm square was measured for each surface and then treated with standardised cut-off lengths (0.08 mm, 0.25 mm and 0.80 mm). Figure 1 indicates the entire process to obtain the roughness in each sample.

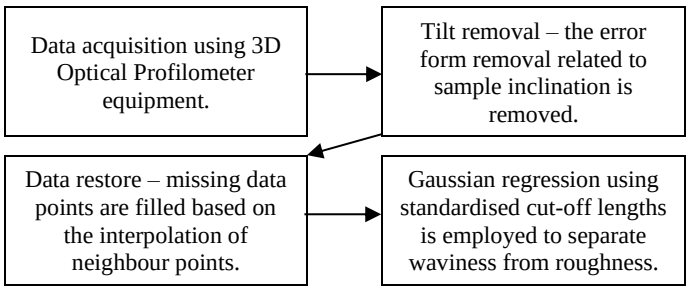

Figure 1 - Data treatment applied to the top-milling surfaces.

For each surface, and considering the three filters, the area parameters S_a, S_q, S_p and S_z were evaluated. Once the surface treatment was performed, it was possible to export the roughness matrix $s(x, y)$ to be employed at the simulations for the respective cut-off length.

4.3 Dry Circular Contact simulation conditions

The DCC simulations assumed a contact between a smooth ball against a rough plane. The parameters used are presented in Table 2. These conditions were used in all simulations, only the roughness matrix changed as the surface and the filters were evaluated. Three different positions were chosen on each surface to position the ball and produce some variability.

4.4 Elastohydrodynamic lubrication simulation conditions

The EHL simulations followed the same analyses introduced for the DCC. The main differences are the ISO VG150 lubricant addition at 40ºC [11] and the entrainment velocity of 2.0 m/s (arbitrarily chosen). The complementary information needed for these simulations is presented in Table 2.

Table 2 – Used parameters for DCC and EHL simulations

Operation conditions	
Parameter	**Value**
Normal Load $(\boldsymbol{P})$	50.0 N
Principal relative radii of curvature $(\boldsymbol{R_x = R_y})$	9.525 mm
Equivalent Young's Modulus $(\boldsymbol{E^*})$	115.385 GPa
Maximum Hertz Pressure $(\boldsymbol{p_h})$	1.124 GPa
Contact radius $(\boldsymbol{a})$	0.146 mm
Entrainment velocity $(\|\vec{\boldsymbol{v}}_e\|)$	2.0 m/s
Lubricant's properties	
Parameter	**Value**
Dynamic viscosity $(\boldsymbol{\eta_T})$ **@** $\boldsymbol{40.0}$℃	0.121 Pa · s
Dynamic viscosity $(\boldsymbol{\eta_T})$ **@** $\boldsymbol{70.0}$℃	0.039 Pa · s
Dynamic viscosity $(\boldsymbol{\eta_T})$ **@** $\boldsymbol{100}$℃	0.016 Pa · s
Lubricant density $(\boldsymbol{\rho_T})$ **@** $\boldsymbol{40}$℃	836.0 kg/m^3
Oil thermal expansion coefficient $(\boldsymbol{\gamma_T})$	$7.53 \cdot 10^{-4}$ ℃$^{-1}$
Pressure-viscosity coefficient $(\boldsymbol{\alpha_{Gold}})$ **@** $\boldsymbol{40.0}$℃	14.341 GPa^{-1}
Other parameters	
Parameter	**Value**
Dimensionless material parameter $(\boldsymbol{G^*})$	3309
Dimensionless speed parameter $(\boldsymbol{U^*})$	$1.100 \cdot 10^{-10}$
Dimensionless load parameter $(\boldsymbol{W^*})$	$2.388 \cdot 10^{-6}$
Mesh node number $(\boldsymbol{N_x = N_y})$	299
$\boldsymbol{\Delta x = \Delta y}$	$3.913 \cdot 10^{-6}$ m

5 Results and analysis

5.1 Roughness results and analysis

Figure 2 presents the four roughness parameters against the feed speed used to manufacture the sample surfaces. The first point to be noticed is that changing the top-milling feed speeds produced different roughness parameters, as expected. Another observed (and predictable) result is the different roughness parameters' sensitivity to the filters. While S_a and S_q present different values and trends with different filters, S_p and S_z do not capture the filtering changes. Still within normal behaviour, reducing the cut-off length led to lower S_a and S_q values [9].

On the other hand, unfortunately, it cannot be said that the top-milling process actually produced three distinct surfaces. The truth is that when looking at the parameters S_a and S_q, which capture surfaces more broadly, the values obtained (in all filters) are very close. For example, looking at the S_a values measured with a 0.80 mm filter, while the lowest roughness is 1.57 µm (900 mm/min), the highest is 2.22 µm (1600 mm/min). This similarity had a significant impact on the maximum pressure prediction.

Another critical aspect in this section is the filtering influence over the distribution of peaks and valleys. As illustrated in Figure 3, the same surface shows quite distinct values. Undoubtedly, this characteristic impacted the simulations and makes clear the need to choose the filter in contact simulations.

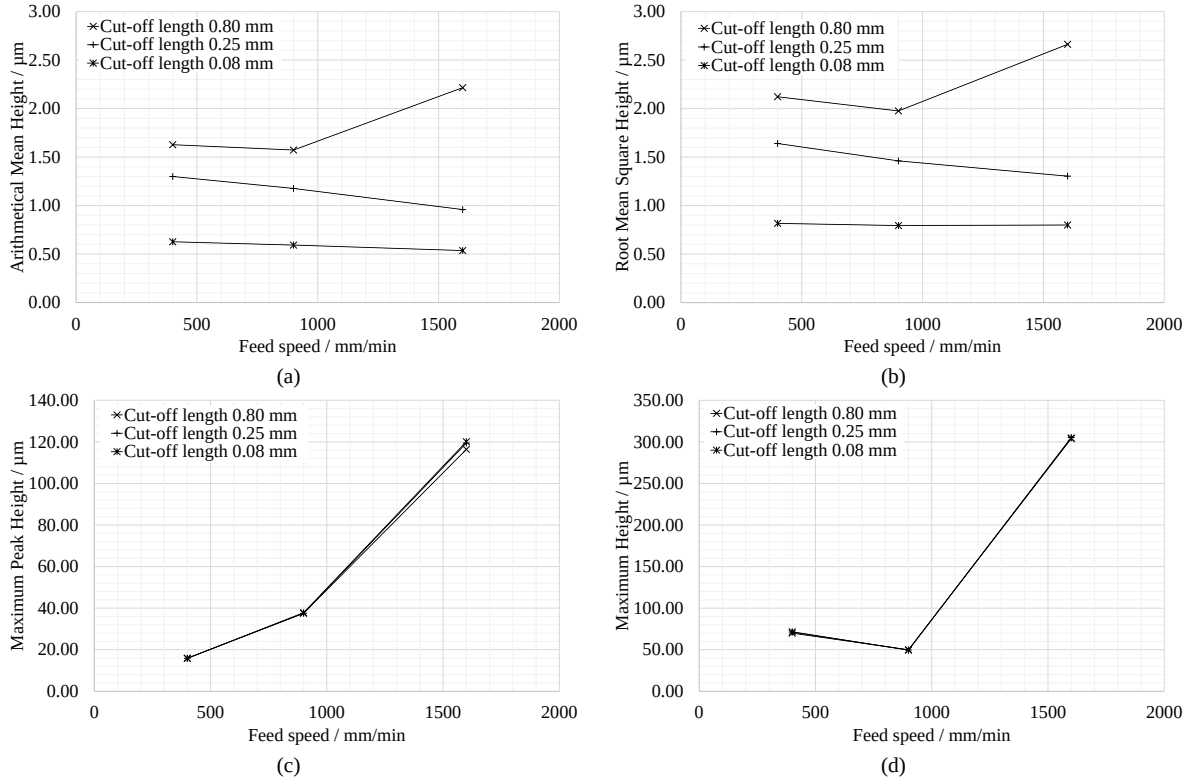

Figure 2 – Roughness parameters against feed speed. (a) Arithmetical Mean Height (S_a), (b) Root Mean Square Height (S_q), (c) Maximum Peak Height (S_p) and (d) Maximum Height (S_z).

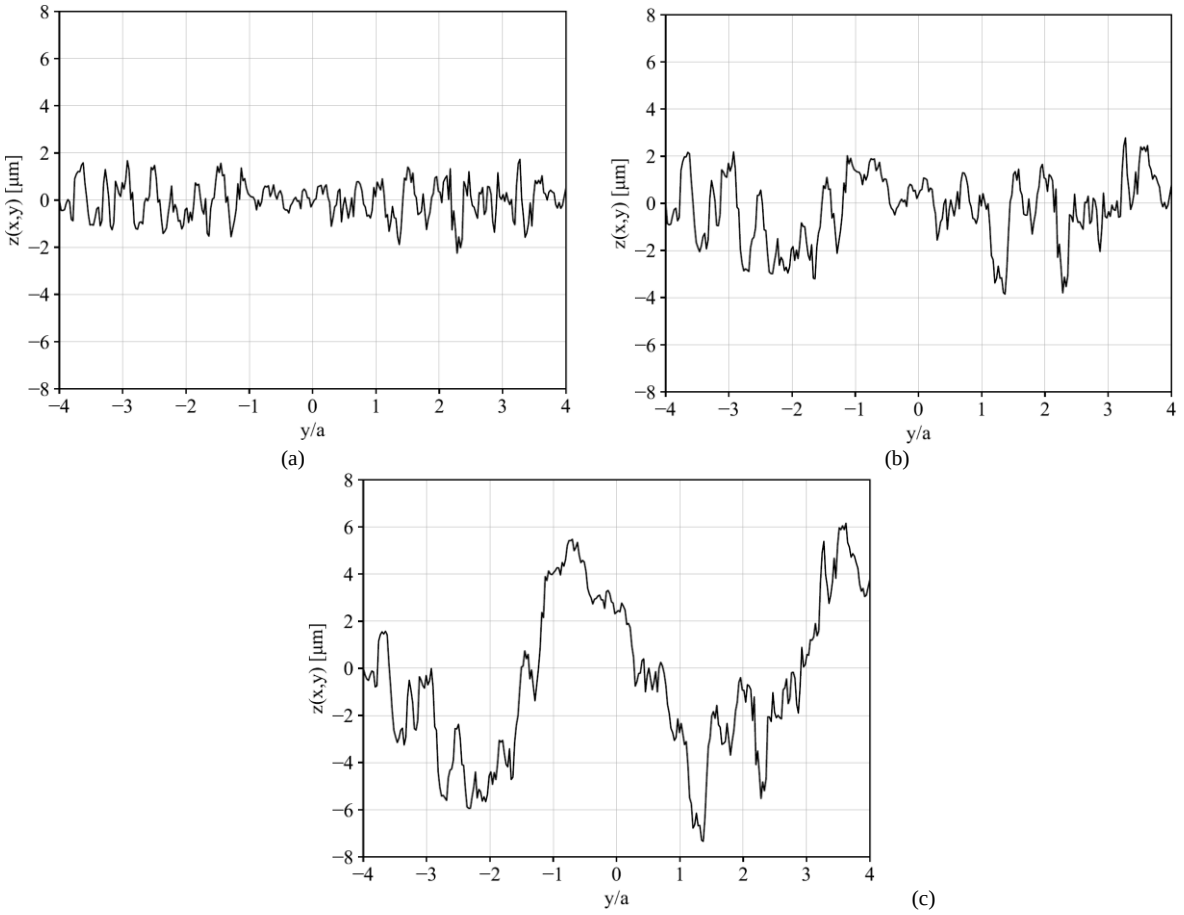

Figure 3 – Filtering influence over the distribution of peaks and valleys. (a) λ_c = 0.08 mm, (b) λ_c = 0.025 mm and (c) λ_c = 0.80 mm.

5.2 Dry Circular Contact results and analysis

Taking three different points on each surface, it was possible to determine an average and a standard error for the maximum contact pressure considering the three mentioned filters. As shown in Figure 4, the maximum pressure results for the DCC simulations were affected by the cut-off length used to generate the surfaces' roughness matrix. In all tested cases, a 0.08 mm filter produced the highest maximum pressure. On the other hand, the dispersion of the results (represented by the standard error bar) was not affected by the filter change.

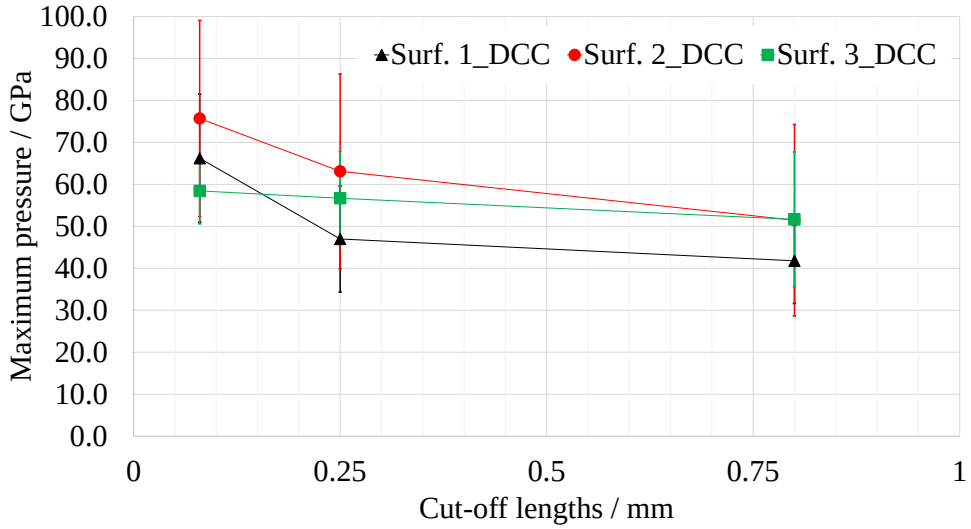

Figure 4 – Maximum pressure average and a standard error for DCC simulations.

5.3 Elastohydrodynamic lubrication results and analysis

The EHL simulations followed the same assumptions presented for DCC. Similarly, Figure 5 shows the maximum pressure results for the EHL simulations, where once more, one can see that the cut-off length also affected the maximum pressure predictions. Again, a 0.08 mm filter produced the highest maximum pressure in all tested cases. However, in this case, the filter also impacted the results' dispersion (represented by the standard error bar), with lower dispersion values for 0.80 mm.

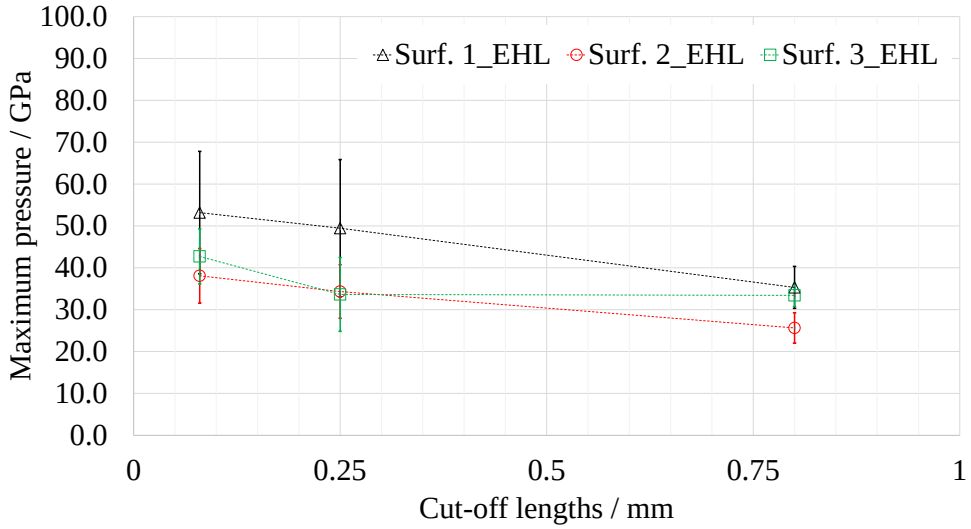

Figure 5 – Maximum pressure average and a standard error for EHL simulations.

An additional comment is that the predicted values with the EHL model were lower than those presented for DCC, which is unsurprising, given that when the lubricant is introduced in the contact, part of the load is supported by it, leading to reductions in contact pressures [11].

5.4 General perceptions

It is essential to acknowledge that the results obtained in this paper were limited by the fact that the three studied surfaces were very similar from the point of view of S_a and S_q (filter-sensitive parameters). The suggested feed speeds for top-milling were expected to lead to surfaces with more significant differentiation. Certainly, other variables pertinent to the machining of the surfaces played a more critical role. In this way, the maximum pressure values obtained for the surfaces, considering any one of the filters, were statistically similar (note that the error bars overlap for the same cut-off lengths). Therefore, it was not viable at this point to establish a clear correlation between the maximum pressures obtained in the simulations and the evaluated roughness parameters S_a, S_q, S_p and S_z. However, this is a particularly interesting topic to be persecuted.

6 Conclusions

This study's results indicate that the filters used to treat the surfaces obtained by optical interferometry indeed influence the maximum pressure obtained in simulations of dry and elastohydrodynamic circular contact. In all simulated cases, an increase in pressure was observed when decreasing the filter length. It is worth indicating to the reader that some care must be exercised here. It is essential to realise that the maximum pressure value, although relevant and very important in the analysis of surfaces, is a punctual representation of what happens on the surface.

On the other hand, the clear perception that the different cut-off lengths produce different pressures for the same surface raises an intriguing question: which filter better represents the actual contact? A more in-depth study seems promising but with a more extensive range of roughness in this case.

Acknowledgements. The authors gratefully acknowledge the financial support of several projects and grants, namely:

- National Funds through Fundação para a Ciência e a Tecnologia (FCT) under the PhD grant 2021.05562.BD;
- National Funds through Fundação para a Ciência e a Tecnologia (FCT) under the PhD grant SFRH/BD/147889/2019;
- LAETA under project UID/50022/2020.

Authorship statement. The authors hereby confirm that they are the sole liable persons responsible for the authorship of this work, and that all material that has been herein included as part of the present paper is either the property (and authorship) of the authors, or has the permission of the owners to be included here.

Nomenclature

a	Hertz contact radius [m]	
A	domain used to analyse the contact area	
$\mathrm{C_a}, \mathrm{C_b}$	coefficients for pressure–density equation	$\mathrm{C_a} = 0.6 \times 10^{-9}$ $\mathrm{C_b} = 1.7 \times 10^{-9}$
E^*	Equivalent Young's modulus [Pa]	$\left(\frac{1-\nu_1^2}{\mathrm{E_1}} + \frac{1-\nu_2^2}{\mathrm{E_2}}\right)^{-1}$
$E_{1,2}$	Young's modulus of bodies 1 and 2 [Pa]	
$h \equiv h(x,y)$	film thickness between bodies 1 and 2 [m]	
h_0	normal approach [m]	
$N_x = N_y$	mesh node number	
P	normal load applied to the contact [N]	
$p \equiv p(x,y)$	pressure distribution [Pa]	
$p(x',y')$	pressure applied at the point $(\mathrm{x}', \mathrm{y}')$ [Pa]	
$R_{x,y}$	principal relative radii of curvature in x, y direction [m]	$\frac{\mathrm{R_{x,y_1}} \cdot \mathrm{R_{x,y_2}}}{\mathrm{R_{x,y_1}} + \mathrm{R_{x,y_2}}}$
$R_{x,y_{1,2}}$	surface principal radii of curvature in x, y direction of bodies 1 and 2 [m]	
$s_{1,2}(x,y)$	surface roughness amplitude of bodies 1 and 2 [m]	
$u_z(x,y)$	pressure-induced elastic displacement at the point (x, y) [m]	
$\lVert\vec{v}_\mathrm{e}\rVert$	entrainment velocity [m/s]	$\frac{\lvert\vec{v}_2 + \vec{v}_1\rvert}{2}$
$\vec{v}_{1,2}$	Velocity of bodies 1 and 2 [m/s]	
x, y	coordinates (x is chosen to be parallel to the rolling direction) [m]	

α_{Gold}	pressure-viscosity coefficient calculated by Gold's formula $[\text{Pa}^{-1}]$
γ_{t}	oil thermal expansion coefficient $[^{\circ}\text{C}^{-1}]$
$\Delta x = \Delta y$	mesh grid size [m]
η	lubricant dynamic viscosity at a given pressure $[\text{Pa} \cdot \text{s}]$
$\nu_{1,2}$	Poisson's Ratio of bodies 1 and 2
ρ	lubricant density at a given pressure $[\text{kg}/\text{m}^3]$
ρ_0	lubricant density at atmospheric pressure and reference temperature $[\text{kg}/\text{m}^3]$
ξ, ζ, ψ	lubricant constants for Voguel equation

References

[1] X. Wang, Y. Liu and D. Zhu. Numerical Solution of Mixed Thermal Elastohydrodynamic Lubrication in Point Contacts With Three-Dimensional Surface Roughness. ASME. J. Tribol. 139(1): 011501. 2017 https://doi.org/10.1115/1.4032963

[2] Q. Wang and D. Zhu. Interfacial Mechanics: Theories and Methods for Contact and Lubrication, CRC Press Taylor & Francis Group, LLC, First Edition, 2019. https://doi.org/10.1201/9780429131011

[3] P. Sainsot and A. Lubrecht. Efficient solution of the dry contact of rough surfaces: a comparison of fast Fourier transform and multigrid methods. Proceedings of the Institution of Mechanical Engineers, Part J: Journal of Engineering Tribology; 225(6), 441 – 448. 2011. https://doi.org/10.1177/1350650111401535

[4] Y. Wang, A. Dorgham, Y. Liu, C. Wang, M. Wilson, A. Neville, A. Azam. An Assessment of Quantitative Predictions of Deterministic Mixed Lubrication Solvers. ASME. J. Tribol. 143(1), 011601. 2021. https://doi.org/10.1115/1.4047586

[5] B. Bhushan. Contact mechanics of rough surfaces in tribology: multiple asperity contact. Tribology Letters. 4, 1–35. 1998. https://doi.org/10.1023/A:1019186601445

[6] C. Barus. Isothermals, isopiestics and isometrics relative to viscosity. American J. of Science 1893, s3-45(266), 87 – 96. https://doi.org/10.2475/ajs.s3-45.266.87

[7] R. Gohar and M. Safa. 5 – Fluid film lubrication. Tribology and Dynamics of Engine and Powertrain, Woodhead Publishing, 2010; 132 – 170. https://doi.org/10.1533/9781845699932.1.132

[8] P. Gold, A. Schmidt, H. Dicke, J. Loos and C. Assmann. Viscosity–pressure–temperature behaviour of mineral and synthetic oils. Journal of Synthetic Lubrication 2006; 18(1), 51 – 79. https://doi.org/10.1002/jsl.3000180105

[9] L. Mummery. Surface Texture Analysis – The Handbook. Hommelwerke GmbH, 106 pages. 1992.

[10] F. Blateyron. The Areal Field Parameters. In: Leach, R. (eds) Characterisation of Areal Surface Texture. Springer, Berlin 2013. https://doi.org/10.1007/978-3-642-36458-7_2

[11] M. J. de M. Cortez. Thermal-Elasto-Plastic-Hydrodynamic Contact Between Rough Surfaces: Influence of Surface Roughness. Master's thesis in Mechanical Engineering, Faculty of Engineering of the University of Porto (FEUP). 2023.